Localization of (photo)respiration and CO₂ re-assimilation in tomato leaves investigated with a reaction-diffusion model

Herman N. C. Berghuijs[1,2,3]*, **Xinyou Yin**[1,2], **Q. Tri Ho**[3], **Moges A. Retta**[1,3], **Pieter Verboven**[3], **Bart M. Nicolaï**[3], **Paul C. Struik**[1,2]

1 Centre for Crop Systems Analysis, Wageningen University & Research, Droevendaalsesteeg 1, Wageningen, The Netherlands, **2** BioSolar Cells, Wageningen, The Netherlands, **3** Flanders Center of Postharvest Technology / BIOSYST-MeBioS, Katholieke Universiteit Leuven, Willem de Croylaan 42, Leuven, Belgium

* herman.berghuijs@wur.nl

Abstract

The rate of photosynthesis depends on the CO₂ partial pressure near Rubisco, C_c, which is commonly calculated by models using the overall mesophyll resistance. Such models do not explain the difference between the CO₂ level in the intercellular air space and C_c mechanistically. This problem can be overcome by reaction-diffusion models for CO₂ transport, production and fixation in leaves. However, most reaction-diffusion models are complex and unattractive for procedures that require a large number of runs, like parameter optimisation. This study provides a simpler reaction-diffusion model. It is parameterized by both leaf physiological and leaf anatomical data. The anatomical data consisted of the thickness of the cell wall, cytosol and stroma, and the area ratios of mesophyll exposed to the intercellular air space to leaf surfaces and exposed chloroplast to exposed mesophyll surfaces. The model was used directly to estimate photosynthetic parameters from a subset of the measured light and CO₂ response curves; the remaining data were used for validation. The model predicted light and CO₂ response curves reasonably well for 15 days old tomato (cv. Admiro) leaves, if (photo)respiratory CO₂ release was assumed to take place in the inner cytosol or in the gaps between the chloroplasts. The model was also used to calculate the fraction of CO₂ produced by (photo)respiration that is re-assimilated in the stroma, and this fraction ranged from 56 to 76%. In future research, the model should be further validated to better understand how the re-assimilation of (photo)respired CO₂ is affected by environmental conditions and physiological parameters.

Introduction

The mesophyll of C₃ plants can substantially constrain CO₂ transport from the intercellular air space to Rubisco[1–4]. This results in a significant drawdown between the CO₂ partial pressures in the intercellular air space (C_i) and near the binding sites of Rubisco (C_c) where CO₂ is fixed. C_c is an input variable for the widely used Farquhar-von Caemmerer-Berry model [5]

(abbreviated as "FvCB model") that is used to predict the net rate of CO_2 assimilation (A_N) of a leaf. In order to calculate C_c, the mesophyll resistance (r_m) to CO_2 transport is commonly introduced as:

$$C_c = C_i - r_m A_N \qquad (1)$$

Fig 1A shows a schematic representation of this model. This approach has several limitations though. r_m, or its inverse (mesophyll conductance g_m), in Eq (1) needs to be estimated by one of the various gas exchange-based methods described in literature (see [6] and [7] for reviews). It has been shown that the mesophyll resistance is not constant, but possibly varies with light and CO_2 levels [8], although there is also proof that part of the variation in r_m with light and CO_2 levels could be caused by measurement errors and statistical artefacts [9,10]. One way to incorporate this variability in Eq (1) is to use a Leuning-type phenomenological model [11] that describes the relation between C_c and g_m [12,13]. However, this approach does not provide a mechanistic explanation for the variability of r_m with light and CO_2 levels.

Recently, a mathematical resistance-model framework [14] was presented to allow for the fact that CO_2 fixation takes place in chloroplasts whereas respiratory and photorespiratory CO_2 (hereafter, (photo)respired CO_2) is released in mitochondria that are in the cytosol. Using this framework, the variability of r_m with CO_2 levels is shown to be at least partly explained by the difference in the diffusion pathway between the (photo)respired CO_2 and the CO_2 coming from the intercellular air space [15]. This model assumes that CO_2 production by (photo) respiration takes place in a cytosol compartment between the plasma membrane and the chloroplast envelope and that there is CO_2 influx from the intercellular air space into this compartment[15]. This implies that CO_2 from the intercellular air space and CO_2 produced by (photo) respiration share the diffusion pathway from the cytosol to Rubisco, where CO_2 is fixed. However, the shared diffusion pathway of these two sources of CO_2 can only occur if one of the following two conditions is met [7,16]. The first condition is that all mitochondria are located between the plasma membrane and the chloroplasts (instead of between the tonoplast and the chloroplasts), as is done in [17] (schematically drawn in Fig 1B). The second condition is that CO_2 in the cytosol is completely mixed as is done in the model described in [14] (schematically Fig 1C). The authors of this model [18] commented on their earlier framework [14] that this latter assumption was made by surmising that the cytosol has a negligible resistance for CO_2 transport. Complete mixture of CO_2 from the atmosphere and CO_2 produced by (photo)respiration implies that CO_2 diffusion in the cytosol is much faster than that in the combined cell wall and plasma membrane and in the chloroplast. Physically, this means that under these assumptions the location of mitochondria does not affect C_c and that this framework cannot be used to investigate the effect of the placement of mitochondria. However, the position of mitochondria relative to the chloroplast may affect net CO_2 assimilation rate. If most of the (photo)respired CO_2 is produced between the chloroplast envelope and the tonoplast, the released CO_2 will likely be re-assimilated. This is especially the case when the space between the chloroplasts is small[19,20]. The exposed mesophyll surface that is not covered by chloroplasts may provide a pathway for CO_2 to escape to the intercellular air space. Overall, it is difficult to mechanistically explain and simulate the variation in r_m with different light and CO_2 levels, using a resistance-model approach.

In order to deal with most of the limitations of the concept of mesophyll resistance and to study the influence of several leaf structural and biochemical properties on leaf photosynthesis separately, reaction-diffusion models of a leaf have been produced. In one of the earliest studies, a leaf was modelled as a porous volume. Within this volume, CO_2 transport and assimilation were simulated [21]. In later studies, the leaf structure was modelled more explicitly to
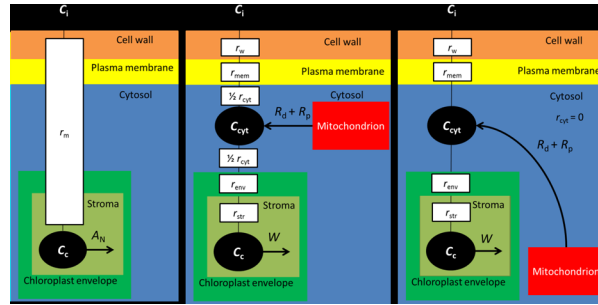
Fig 1. Schematic representation for the different types of models for the resistance of CO$_2$ transport in the mesophyll. The C_i, C_{cyt} and C_c represent the CO$_2$ partial pressure in the intercellular air space, the cytosol and the CO$_2$ binding cites of Rubisco in the chloroplast stroma, respectively. In the model in Panel A), all structural barriers of the mesophyll for CO$_2$ transport are lumped in a single resistance, called mesophyll resistance r_m. The intracellular sinks and sources for CO$_2$ are assumed to be at the same location, i.e. in the chloroplast stroma. The net flux of CO$_2$ from the chloroplast stroma equals the net CO$_2$ assimilation rate A_N. In the model in Panel B) an additional cytosol compartment is added. The resistance components for CO$_2$ transport between the air spaces and this compartment is the sum of resistances of the of the cell wall (r_w), of the plasma membrane (r_{mem}) and half the resistance of the cytosol (r_{cyt}). The resistance components for CO$_2$ transport between the cytosol compartment and Rubisco consists of the resistance of the chloroplast envelope (r_{env}) and the CO$_2$ diffusion path in the stroma (r_{str}). The rate of carboxylation by Rubisco (W) in the chloroplast stroma is the sink for CO$_2$. The intracellular sources of CO$_2$ are the rate of respiration in the light (R_d) and the rate of photorespiration (R_p). Both sources are located in the cytosol. This model places the source for CO$_2$ between two cytosol resistance components and can, therefore, only be used to study C$_3$ leaf photosynthesis if the mitochondrion are located in the outer cytosol layer. The model in Panel c) is largely similar to the model in Panel C), with the exception that the resistance of the cytosol is negligible. Consequently, the CO$_2$ partial pressure is equal in any part of the cytosol and C_{cyt} is not affected by the location of the mitochondrion relative to the chloroplast. Therefore, this model cannot be used to study how the position of the mitochondria relative to the chloroplast affects C$_3$ leaf photosynthesis.

study the effect of stomatal opening state and pore size, gradients of CO$_2$ in the intercellular air space [22–24], and the effect of temperature dependency of carbon anhydrase activity, CO$_2$ solubility and diffusion-related related parameters [23,25,26] on CO$_2$ assimilation. A limitation of these models is that they assume that (photo)respiration and CO$_2$ assimilation take place in the same compartments. More recent reaction-diffusion models [27,28] describe the structure in more detail in order to compartmentalize these processes, allowing mechanistic modelling of the contribution of (photo)respired CO$_2$ to the calculated mesophyll resistance. There has also been a resistance model that tried to achieve this [17]. This model calculated the resistance of each mesophyll component by dividing the length of the diffusion path of these components by their diffusion coefficient as described in [29]. These lengths can be determined as the thickness of the compartment in the cases of the cell wall and the cytosol. However, this cannot be done to quantify the diffusion pathway length in the stroma, as CO$_2$ is consumed along its diffusion path in the stroma. Therefore, the average diffusion path of a CO$_2$ molecule in the stroma is shorter than the stroma thickness. This issue can be tackled by calculating the diffusion path length as the product of the stroma thickness and a fixed fraction, as previously described in [29]. However, the value of this fixed fraction is unknown and sensitivity analyses showed that the net CO$_2$ assimilation rate calculated by this type of model is very sensitive to this parameter[17]. Compared with resistance models [17,29,30] that use anatomical properties to calculate r_m and C_c, reaction-diffusion models do not require a predefined diffusion distance in the chloroplasts.

Recently, a 3-D reaction-diffusion model for CO$_2$ and HCO$_3^-$ transport was implemented into a detailed representation of a single mesophyll cell[27]. Another recent model [28] also described CO$_2$ and HCO$_3^-$ transport, but incorporated the geometry of leaf tissue based on

synchrotron computed laminography images. The complexity of these computational domains has consequences. The model in [27] describes a very detailed cell microstructure. Therefore, it may become computationally expensive if a whole mesophyll tissue sample is modelled in this way. The computationally expensive models are unattractive to use for procedures that require a large number of model runs, like optimization or parameter estimation. When running this model (assuming a constant light absorption throughout the leaf) to simulate a CO_2 response curve on a personal computer (Processor Intel(R) Xeon CPU W3550 @ 3.07 GHz 3.06 GHz, Installed memory: 24 GB RAM), it took us about 9 hours to simulate a single point in a CO_2 response curve and several days to simulate the whole curve. Although this can be speeded up by the use of parallel computing, it still takes several hours before the simulation of a single curve is completed. Also, the 3-D leaf geometry in [28] is a direct reconstruction of a whole leaf section, which makes it impossible to change the structure of mesophyll cells for sensitivity analyses.

In the current study, we present a simple 2-D microstructural model of a leaf, in which CO_2 transport, CO_2 production by (photo)respiration, and CO_2 consumption by carboxylation are modelled. The mesophyll microstructures in the model are very simple and flexible. This makes the model easy to apply to a wide range of C_3 species within a reasonable computational time. The model will be parameterized from simultaneously measured data for gas exchange and chlorophyll fluorescence. We will demonstrate that the model can contribute to the understanding of how the position of the sites of mitochondria relative to the chloroplast stroma affects the re-assimilation of CO_2 produced by (photo)respiration, and thus, the net rate of CO_2 assimilation.

Results

Overall description of the model

The model consists of two main parts: a description of the geometry of the computational domain and a mathematical formulation, in the form of partial differential equations and boundary conditions, of the processes that are simulated within this geometry.

The computational domain consists of a rectangular section (Fig 2). This section contains a single rectangular chloroplast surrounded by a layer of cytosol. CO_2 enters the domain by diffusing through the cell wall and plasma membrane into the outer cytosol. From there, it diffuses through the double-layered chloroplast membrane into the stroma. Part of the CO_2 may diffuse through cytosol gaps between the chloroplasts and enter the inner cytosol. CO_2 may be produced through (photo)respiration in the outer cytosol, or the inner cytosol or the cytosol gaps between the chloroplasts, depending on where mitochondria are located. (Photo)respired CO_2 either escapes towards the intercellular space, or diffuses back into the chloroplasts, being re-assimilated. The construction and the parameterization of the computational domain (Fig 2) are described in S1 Text and S2 Text, respectively.

CO_2 transport, CO_2 production by (photo)respiration, and CO_2 consumption by RuBP carboxylation were simulated by solving a reaction-diffusion model over this domain. The partial differential equations and the boundary conditions were parameterized by both leaf anatomical properties and simultaneous gas exchange and chlorophyll fluorescence measurements. Table 1 shows an overview of definitions and values of all model parameters and input variables. Thicknesses of the cell wall (t_{wall}), cytosol (t_{cyt}), and the chloroplast stroma (t_{str}) were adopted from[17], in which they were measured from transmission electron microscopic photographs of tomato (*Solanum lycopersicum*) mesophyll cells. The ratios of the mesophyll surface area exposed to the intercellular air space to the leaf surface (S_m/S) and the chloroplast surface area facing the intercellular air space to the exposed mesophyll surface area (S_c/S_m)

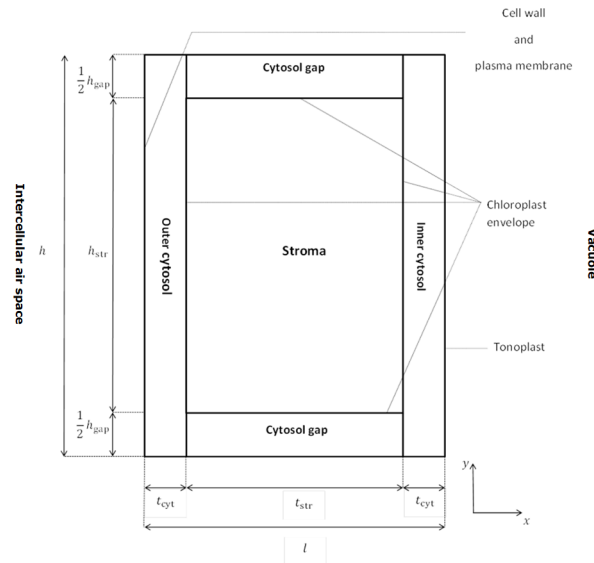**Fig 2. Schematic drawing of the computational domain and its position relative to the intercellular air space and the vacuole.**

https://doi.org/10.1371/journal.pone.0183746.g002

were adopted from measurements presented in the same study. The Michaelis-Menten constants for RuBP carboxylation (K_{mC}) and for oxygenation (K_{mO}) were adopted from[28], who estimated these parameters using data from simultaneously conducted gas exchange and chlorophyll fluorescence measurements on tomato leaves. Also, the diffusion coefficients and permeabilities of the various mesophyll components were adopted from this study.

Input FvCB parameters that represent partial pressure were converted from Pa to mol m^{-3}. Input parameters that represent rates expressed in μmol m^{-2} s^{-1} were converted to mol m^{-3} s^{-1}. After solving the model, the average rate of CO_2 assimilation (mol m^{-3} s^{-1}) in the chloroplast was calculated from the steady state CO_2 distribution. It was used to calculate the rate of CO_2 assimilation at the leaf level, expressed in μmol m^{-2} s^{-1}. The Material and Methods section and S3 Text contain more information about these unit conversions.

Estimates of R_d, T_p, and V_{cmax}

We estimated s, which is the slope of the assumed linear relationship between J and $I_{inc}\Phi_2/4$ at low light levels and low O_2 levels using the method described in[13]. We used this parameter, the average measured quantum yield of photosystem II, and the irradiance to calculate the rate of electron transport (Eq 8). After determination of s, the rate of respiration R_d and the maximum rate of RuBP carboxylation V_{cmax} were estimated by the 2-D model. Table 2 shows R_d and V_{cmax} and their standard errors estimated by our model. The estimate of s was 0.529. The estimates for R_d were 3.43 μmol m^{-2} s^{-1}, 3.36 μmol m^{-2} s^{-1}, and 3.41 μmol m^{-2} s^{-1} assuming the (photo)respired CO_2 is released in the inner cytosol, the outer cytosol and the cytosol gap compartments, respectively. These R_d and the measured A_j values were used to calculate T_p, which was 13 μmol m^{-2} s^{-1} for each assumed location of (photo)respiration (Table 2). The estimates of V_{cmax} were 174 μmol m^{-2} s^{-1}, 177 μmol m^{-2} s^{-1}, and 227 μmol m^{-2} s^{-1} assuming (photo)respiratory CO_2 release in the inner cytosol, the outer cytosol and the cytosol gaps, respectively. Those estimates of R_d are considerably higher than the ones reported in [7,28] for young cv. Admiro leaves. In both studies, the Yin method [13] was used to estimate R_d as the intercept of the correlation between A_N and $I_{inc}\Phi_2/4$ for high atmospheric CO_2 partial pressures and very

Table 1. Values of parameters and variable input for the model.

Symbol	Explanation	Value	Unit	Source
C_a	Ambient CO_2 partial pressure near leaf surface	*	Pa	[17]
$D_{CO2, water}$	Diffusion coefficient of CO_2 in water at $T = 298.13$ K	$1.79 \cdot 10^{-9}$	$m^2 s^{-1}$	[29]
g_s	Stomatal conductance	**	$mol\ m^{-2} s^{-1}$ Pa^{-1}	[28]
G_{mem}	Plasma membrane permeability	$3.50 \cdot 10^{-3}$	$m\ s^{-1}$	[17]
G_{env}	Chloroplast envelope permeability	$1.75 \cdot 10^{-3}$	$m\ s^{-1}$	[28]
H	Henry's constant for CO_2 at $T = 298.13$ K	2941	$Pa\ m^3 mol^{-1}$	[17]
I_{inc}	Irradiance	*	$\mu mol\ m^{-2} s^{-1}$	
K_{mC}	Michaelis-Menten constant for RuBP carboxylation by Rubisco	26.7	Pa	[28]
K_{mO}	Michaelis-Menten constant for RuBP oxygenation by Rubisco	16.4	kPa	[28]
O	Oxygen partial pressure	21	kPa	
$p_{eff,wall}$	Effective porosity of the cell wall	0.2		[17]
q	Ratio of the height of a chloroplast to its thickness	2.5		[27]
R	Universal gas constant	8.314	$Pa\ m^3 mol^{-1}$ K^{-1}	[17]
R_d	Rate of respiration in the light	***	$\mu mol\ m^{-2} s^{-1}$	
s	Slope of the assumed linear relationship between J and $I_{inc}\Phi_2/4$ at low light levels and low O_2 levels	0.529		
S_m/S	Ratio of the area of the mesophyll cell surface, exposed to the intercellular air space, to the leaf surface area	17.0		[17]
S_c/S_m	Ratio of the area of the chloroplast surface, facing the intercellular air space, to the mesophyll surface area, exposed to the intercellular air space	0.919		[17]
$S_{C/O}$	Rubisco specificity factor	2.6	$mmol\ \mu mol^{-1}$	[14]
t_{wall}	Cell wall thickness	0.118	μm	[17]
t_{cyt}	Cytosol thickness	0.243	μm	[17]
t_{str}	Stroma thickness	2.54	μm	[17]
T	Leaf temperature	298.13	K	
T_p	Rate of triose phosphate utilization	***	$\mu mol\ m^{-2} s^{-1}$	
V_{cmax}	Rate of RuBP carboxylation by Rubisco	***	$\mu mol\ m^{-2} s^{-1}$	
ζ_{cyt}	Fraction of CO_2 diffusion coefficient in cytosol to CO_2 diffusion coefficient in water	0.5		[28]
ζ_{str}	Fraction of CO_2 diffusion coefficient in stroma to CO_2 diffusion coefficient in water	0.5		[28]
Φ_2	Quantum yield of photosystem II	**	$mol\ mol^{-1}$	[28]

* Environmental conditions; during the gas exchange and chlorophyll fluorescence measurements, the leaf was exposed to various combinations of C_a, I_{inc}, and O.

** For each combination of C_a and I_{inc}, g_s and Φ_2 were measured.

*** These parameters were estimated by the model for different scenarios for the location of (photo)respiration.

https://doi.org/10.1371/journal.pone.0183746.t001

low oxygen levels. Possibly, the differences between our and their estimates is that the Yin method, which, strictly speaking, applies to non-photorespiratory conditions [17], was used to

Table 2. Estimated values of parameters of the FvCB model and their standard error for each scenario for (photo)respired CO_2 release (it takes place in the inner cytosol, or in the outer cytosol, or in the cytosol gaps).

Symbol	Unit	Explanation	(Photo)respired CO_2 release in:		
			Inner cytosol	Outer cytosol	Cytosol gaps
R_d	$\mu mol\ m^{-2} s^{-1}$	Rate of respiration	3.44±0.36	3.36±0.36	3.41±0.36
T_p	$\mu mol\ m^{-2} s^{-1}$	Rate of triose phosphate utilization	13.39	13.38	13.38
V_{cmax}	$\mu mol\ m^{-2} s^{-1}$	Rate of RuBP carboxylation by Rubisco	174±29	177±251	227±29

https://doi.org/10.1371/journal.pone.0183746.t002

estimate R_d under ambient oxygen levels in their study. In contrast, our model does not have such a restriction and the estimate by our model should better represent R_d under ambient O_2 levels. In order to investigate to what extent our relatively high R_d estimates could have influenced our estimates for V_{cmax}, we estimated V_{cmax} for a range of R_d values varying from 1.0 µmol m^{-2} s^{-1} to 5.0 µmol m^{-2} s^{-1} (Table A in S9 Text). The estimate of V_{cmax} was not effected by R_d if (photo) respired CO_2 is released in the outer cytosol and that the standard error of the estimate was very high relative to the estimate. In the other two scenarios, the standard error of the estimates was small relative to the estimate. The estimates of V_{cmax} increased with the assumed values of R_d. However, the relative increase of the estimated V_{cmax} with increasing R_d was relatively small as an increase of R_d by 500% only resulted in an increase of V_{cmax} by 18% and 24% for the scenarios that assume (photo)respiratory CO_2 release in the inner cytosol and cytosol gaps, respectively.

In order to compare the estimates and the standard errors of V_{cmax} found by our model and by the FvCB model extended with mesophyll conductance, we estimated V_{cmax} using the estimation procedure described in[13], which assumes [11] that mesophyll conductance varies with C_i according to a Leuning-type phenomenological model[11]. The SAS 9.4 script (SAS Institute Inc., Cary, NC, USA) for this procedure can be found in Script A in S10 Text. We set in this analysis that R_d = 3.4 µmol m^{-2} s^{-1}, which is the average of the estimated R_d across the three scenarios (Table 2). We used the same experimental data for those low CO_2 levels as we used for the estimation of V_{cmax} using the 2-D model. This analysis resulted in an estimate of V_{cmax} = 130 ± 19 µmol m^{-2} s^{-1}, which was simultaneously estimated with shape parameter δ (5.7486±3.4596)[11–13]. The standard error of V_{cmax} is of the same order of magnitude as the estimates by the 2-D model, which that assumes (photo)respired CO_2 release in the inner cytosol and the cytosol gaps, but the estimate is smaller than any of the scenarios investigated by the 2-D model (Table 2). This lower estimated value may be explained by the fact that we had to estimate V_{cmax} simultaneously with shape parameter δ to take the variation of mesophyll conductance with C_i into account. In contrast, it was not necessary to estimate such an additional parameter with the 2-D model presented in this study.

Validation

Fig 3 shows a comparison between the simulated and measured net CO_2 assimilation rates. Only the lower parts of the A_N-I_{inc} curve ($I_{inc} \leq 200$ µmol m^{-2} s^{-1}) were used for the estimation of photosynthetic parameters of s and R_d. Only the measurements at C_a = 200 Pa in the A_N-C_a curve were used to determine T_p. The model was validated by predicting A_N for the remaining levels of C_a and I_{inc} that were used in the experiment. If (photo)respired CO_2 is released in the inner cytosol, the model predictions of A_N generally agree well with the measurements. The same is true if (photo)respired CO_2 release is assumed to take place in the cytosol gap compartment, although the model tends to slightly underestimate A_N for intermediate C_a levels in the A_N-C_a curve. This underestimation is considerably higher if (photo)respired CO_2 is assumed to take place in the outer cytosol (Fig 3B and 3C). Additionally, if $I_{inc} \geq 200$ µmol m^{-2} s^{-1}, the predicted A_N is substantially lower than the measured A_N, if (photo)respiratory CO_2 release takes place in the outer cytosol (Fig 4).

CO_2 concentration profiles

Figs 5–7 show CO_2 concentration profiles at ambient CO_2 levels (C_a = 40 Pa) and saturating light (I_{inc} = 1500 µmol m^{-2} s^{-1}) for three scenarios. It is assumed that (photo)respiratory CO_2 is released in the inner cytosol (Fig 5), in the outer cytosol (Fig 6) or in the cytosol gaps (Fig 7). If CO_2 is released in the outer cytosol, the CO_2 partial pressure decreases along the diffusion
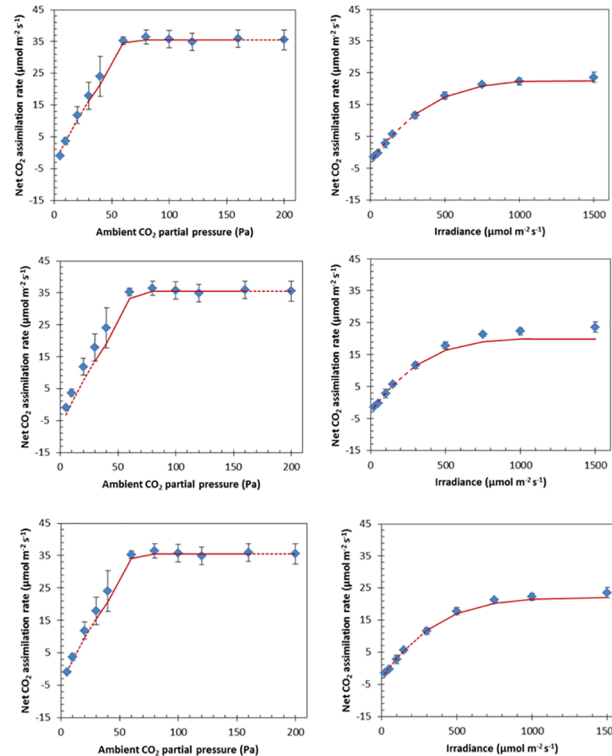
Fig 3. Measured (symbols) and simulated (lines) A_N-C_a (left) and A_N-I_{inc} (right) curves for different scenarios for the location of (photo)respiratory CO₂ release. The error bars represent one standard deviation. In the simulated A_N-C_a curves, (photo)respiration either takes place in the inner cytosol (A-B), in the outer cytosol (C-D) or in the cytosol gaps (E-F). The solid line represents the predicted net CO₂ assimilation rates for values of C_a and I_{inc} that were neither used in the estimation procedure of R_d and V_{cmax} nor for the determination of T_p. The dashed lines connect the predicted net CO₂ assimilation rates under the remaining values of C_a and I_{inc} with the solid curve.

pathway from the cell wall to the tonoplast. If CO₂ is released in the inner cytosol or in the cytosol gap, the CO₂ partial pressure also decreases along the diffusion pathway from the cell wall to near the inner chloroplast envelope. However, in these two scenarios, it slightly increases again in the inner cytosol (Figs 5 and 7).

Re-assimilation of CO₂

The reaction-diffusion model was used to calculate the fraction of re-assimilation of CO₂ produced by (photo)respiration, f_{rec}. It was calculated under ambient CO₂ levels (C_a = 40 Pa) and saturating light (I_{inc} = 1500 μmol m⁻² s⁻¹). The highest values for f_{rec} were obtained if (photo) respired CO₂ release took place in the inner cytosol (f_{rec} = 0.76), The lowest values of f_{rec} were obtained if it took place in the outer cytosol (f_{rec} = 0.56). If it took place in the cytosol gap, f_{rec} = 0.70. The reaction-diffusion model was also used to calculate the average CO₂ partial pressure C_c in the stroma, expressed as a gas phase concentration, for each of the different scenarios. The highest value for C_c was found if (photo)respired CO₂ release took place in the inner cytosol (C_c = 15.6 Pa), and the lowest value for C_c was found if (photo)respired CO₂ release took place in the outer cytosol (C_c = 14.1 Pa). If (photo)respired CO₂ release took place in the cytosol gaps, C_c was 15.1 Pa. The calculated values for the CO₂ partial pressure in the intercellular air spaces were 26.0 Pa, 27.5, and 26.5 Pa for the three scenarios, respectively.
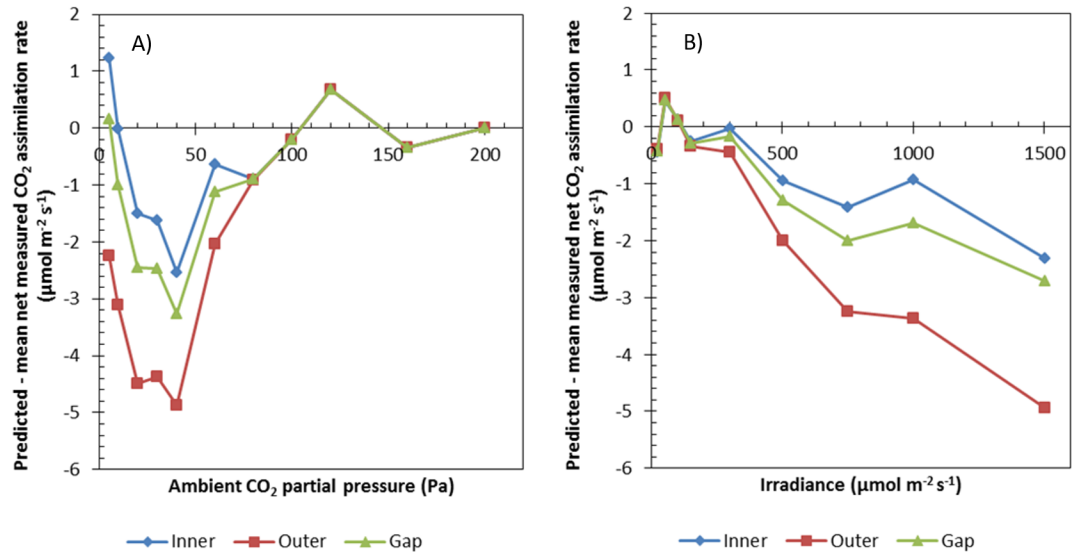
Fig 4. Differences between predicted and measured net CO$_2$ assimilation rates. Differences between the predicted net CO$_2$ assimilation rate and the average measured net CO$_2$ assimilation rate for different ambient CO$_2$ partial pressures (A) and irradiances (B). In both figures, it is assumed in models that (photo)respired CO$_2$ is released in the inner cytosol, or in the outer cytosol, or in the gaps between the inner and the outer cytosol.

Discussion

In this study, a 2-D microstructural model for photosynthesis was developed based on a simplified geometry of a mesophyll cell consisting of four compartments (outer cytosol, chloroplasts, inner cytosol, cytosol gaps) (Fig 2). The microstructural model was parameterized by

Fig 5. CO2 concentration profiles for (photo)respiratory CO2 release in the inner cytosol. CO$_2$ partial pressure profile within half the computational domain at C_i = 25 Pa levels and saturating light (I_{inc} = 1500 μmol m^{-2} s^{-1}). The color bar displays CO$_2$ partial pressures (Pa). (Photo)respired CO$_2$ is produced in the inner cytosol.
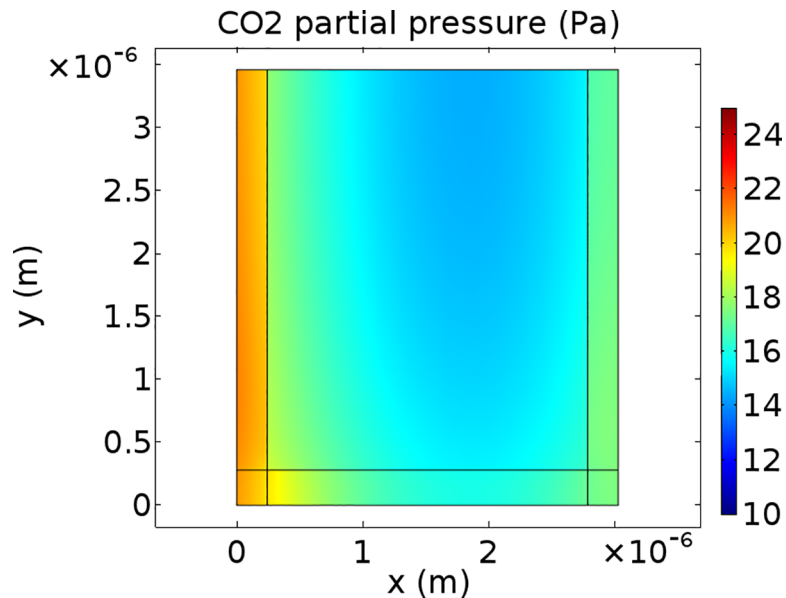
Fig 6. CO2 concentration profiles for (photo)respiratory CO2 release in the outer cytosol. CO$_2$ partial pressure profile within half the computational domain at C_i = 25 Pa levels and saturating light (I_{inc} = 1500 μmol m^{-2} s^{-1}). The color bar displays CO$_2$ partial pressures (Pa). (Photo)respired CO$_2$ is produced in the outer cytosol.

the measured leaf anatomical properties S_c/S_m, t_{cyt}, and t_{str} (Table 1), which were determined from transmission electron microscopic images [17], and an assumed value for the aspect ratio of a chloroplast. Within the microstructural model, a reaction-diffusion model was solved for
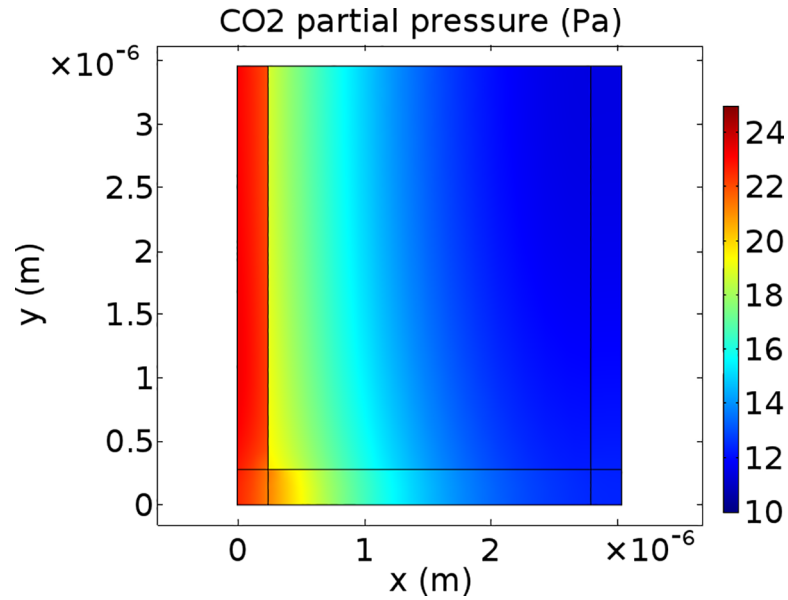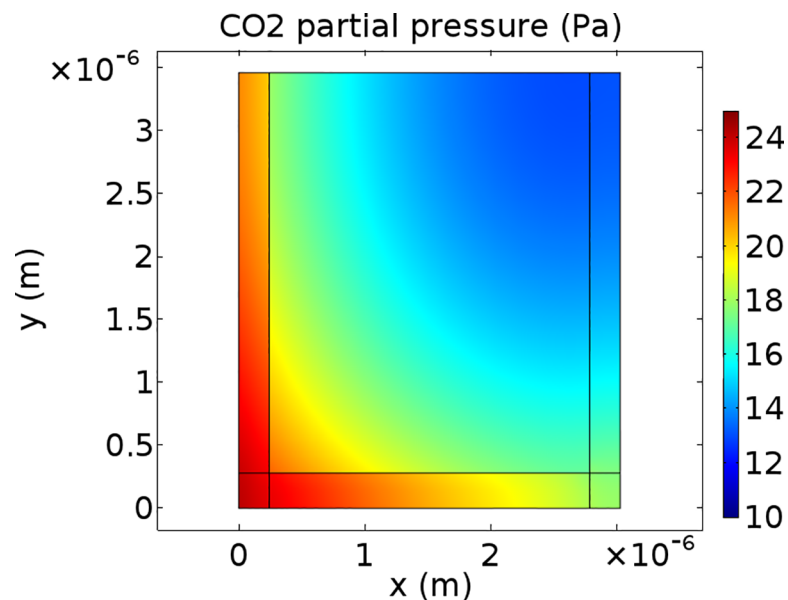

Fig 7. CO2 concentration profiles for (photo)respiratory CO2 release in the cytosol gaps. CO$_2$ partial pressure profile within half the computational domain at C_i = 25 Pa levels and saturating light (I_{inc} = 1500 μmol m^{-2} s^{-1}). The color bar displays CO$_2$ partial pressures (Pa). (Photo)respired CO$_2$ is produced in the cytosol gaps.

CO_2. The model was used directly to estimate the parameters R_d and V_{cmax} for each scenario of (photo)respired CO_2 release.

By estimating R_d with the model, the estimation method does not make the assumption that there is no re-assimilation of (photo)respired CO_2, which is made implicitly in simpler models to estimate R_d [13,31–34]. Current models for mesophyll resistance models either made the implicit assumption that CO_2 release by (photo)respiration takes place in the stroma itself [3,13,35,36], in the outer cytosol [17] or that there is no CO_2 gradient in the cytosol [14,18]. By estimating V_{cmax} with the 2-D model, the estimation method also avoids the assumption that (photo)respiration and RuBP carboxylation take place in the same compartment or that the location of (photo)respiration is limited to the outer cytosol.

The model was validated by comparing the predicted A_N with measurements for A_N that were not used for estimation of R_d and V_{cmax} or the determination of T_p (Fig 3). The model described the data well for both the light and the CO_2 response curves, if it was assumed that (photo)respiratory CO_2 release takes place in the inner cytosol. In the other two simulated cases for the location of (photo)respiration (outer cytosol and cytosol gap), the model tended to predict lower values for the net CO_2 assimilation rate for high light levels and/or low CO_2 levels. The estimates of R_d did not differ among the scenarios for the localizations of (photo)respiration (Table 2). The estimate of V_{cmax} for the scenario that assumes release of (photo)respired CO_2 in the cytosol gaps is higher than in the scenario that assumes release of (photo)respired CO_2 in the inner cytosol (Table 2). An explanation for the difference between the V_{cmax} estimates is that the model in the latter scenario attempts to compensate the short diffusion path for (photo)respired CO_2 with a more efficient RuBP carboxylation. This does not explain why the estimate of V_{cmax} in the scenario for (photo)respired CO_2 release in the outer cytosol is lower than the estimate than in the scenario that assumes (photo)respired CO_2 release in the cytosol gaps though. The very high standard error in the scenario of the model that assumes (photo)respired CO_2 release in the outer cytosol suggests that the estimate of V_{cmax} in this scenario is very uncertain. This uncertainty can either be explained by the absence of Rubisco limited photosynthesis in the data range that was used to estimate V_{cmax} or by an inability of the model to compensate the short length of the diffusion path for (photo)respired CO_2 by estimating a higher V_{cmax} value. Given the poorer performance of the scenario assuming (photo)respiratory release in the outer cytosol during the model validation compared to the other two scenarios (Fig 4), the latter explanation is more likely. These results suggest that CO_2 release by (photo)respiration is more likely to take place in the inner cytosol or the cytosol gaps than in the outer cytosol.

Our results also show that the estimates of R_d are very little affected by the localization of (photo)respiration. This is in contrast with the results from the study in [37]. In that study, a slope-regression method was combined with the multiple resistance model from [14,18] to estimate R_d simultaneously with Γ^*, while assuming different ratios of r_w (serial resistance of cell wall and plasma membrane) and r_c (serial resistance of the chloroplast envelope and the stroma). It was found in that study that changing the assumed ratio of r_c and r_w from 0 to 1 resulted in a decrease of the estimate of R_d by 30%. The fact that we did not find such a change in the estimate in our study may be explained by the fact that R_d was not estimated simultaneously with Γ^*. We did find that the estimate of V_{cmax} was affected by the localization of (photo)respiratory CO_2 release, as its estimates differed considerably among the scenarios. The results from [37] and our results show that it is possible that the assumptions about the localization of (photo)respiratory can affect the estimates of other parameters of the FvCB model and further research is needed to examine this.

After validation, the model was extended to allow simulating the transport, consumption and production of $^{12}CO_2$ and $^{13}CO_2$ simultaneously. This approach allowed us to implement

in silico experiments to determine the percentage for re-assimilation of CO$_2$ produced by (photo)respiration. Our results show that the re-assimilation percentage varied from 56% to 75%, depending on the scenario. The range of reported values for f_{rec} in literature is large. In one study, it is determined that 23%-29% of the (photo)respired CO$_2$ is recycled [38]. However, this percentage is likely underestimated, because the authors assumed in their calculations that the ratio of the concentrations ^{12}CO$_2$ to ^{13}CO$_2$ in the intercellular air space is the same as in the chloroplasts, which is very unlikely[28]. In another study, a resistance model was used [14] to calculate that this percentage is between 25% and 40% in tobacco. However, in that study it was assumed that the CO$_2$ concentration is completely mixed throughout the cytosol. Results from our study clearly show that this is not the case (Figs 5–7). It has also been reported that 100% of the (photo)respired CO$_2$ is re-assimilated in tomato and over 80% is re-assimilated in a number of other species [39]. In another study, re-assimilation percentages were found to be between 14% and 18% in sunflower and rye and between 42% and 50% in wheat[35]. More recently, a somewhat higher re-assimilation percentage has been reported for wheat (45.9%) under an ambient CO$_2$ level [20]. Under a lower CO$_2$ level (200 µmol mol^{-1}), this percentage was about the same (i.e. 46.8%). In the same study, it has been observed that 50.6% of the (photo)respired CO$_2$ is re-assimilated in rice under ambient CO$_2$ level. However, in contrast to wheat, the re-assimilation percentage was considerably higher under low CO$_2$ levels in rice (58.7%). This literature overview shows that the range of possible values for f_{rec} is considerable, even within species, and that the use of different environmental conditions, and species and methods affects the calculated or measured value of f_{rec} and that f_{rec} can even be different within species. In future research, our model can be used to determine f_{rec} for different species or environmental conditions to examine how differences between re-assimilation fractions between species can be explained.

An advantage of the 2-D model presented in our study is that it does not require determining mesophyll resistances, because several factors that determine mesophyll resistance are explicitly modelled. However, the model requires a number of assumed values of diffusion coefficients and permeabilities of several mesophyll cell compartments. The permeability of both the plasma membrane and the chloroplast envelope was adopted from [17]. We assumed that this permeability lumps the permeability for CO$_2$ of aquaporins and the phospholipid bilayer in these membranes [40]. We also assumed that the permeability of the chloroplast envelope is twice as low as the plasma membrane. Values for the effective porosity of the cell wall $p_{eff,wall}$ were adopted from [41] and effective diffusion coefficients from the stroma and cell wall from [28]. Since there are only a very few measurements of these diffusive properties and permeabilities available [42], it can be argued that these uncertainties can result in large errors in the predicted net CO$_2$ assimilation rate. Nevertheless, validation of the model showed that the model predicted the net CO$_2$ assimilation rate reasonably well for both the case that (photo)respiration takes place in the inner cytosol (Fig 3A and 3B) and in the cytosol gap (Fig 3E and 3F). This suggests that even though each single assumed permeability or diffusion coefficient can be biased, the combination of these assumptions results in reasonable predictions of light and CO$_2$ response curves.

Compared with other recent reaction-diffusion models for CO$_2$ transport in leaves [27,28], we made a number of simplifications in both the modelled leaf structure and in the processes. These simplifications are as follows. (i) The compartment in which (photo)respiratory CO$_2$ is released is a compartment in which mitochondria and cytosol are lumped, rather than modelling individual mitochondria as described in [27]. (ii) It is assumed that the resistance of the intercellular air space is negligible, rather than explicitly model the intercellular air space like in[28]. (iii) The leaf model is 2-D, instead of 3-D as was done in previous studies[27,28]. (iv) The leaf structure is reduced to simple geometrical shapes. (v) The light absorption gradient is

not explicitly modelled like in [28,43]. (vi) The activity of carbonic anhydrases is lumped in the apparent diffusion coefficient of the stroma and the cytosol, rather than modelling its activity and HCO$_3^-$ transport explicitly. We have made these simplifications, because adding more complexity requires additional assumed parameter values that are uncertain and cannot easily be measured. Adding complexity will also make the model less flexible and more computationally demanding, which makes the model cumbersome and unattractive to use. Nevertheless, any of these simplifications can potentially have a substantial impact on the predictions. We, therefore checked how these simplifications might affect the predicted net CO$_2$ assimilation rate. We investigated simplification (i) in S4 Text where we presented a modified version of the model in which we modelled individual mitochondria explicitly and compared the predicted net CO$_2$ assimilation rate and f_{rec} with the predictions of the default model. We found that modelling loose mitochondria hardly changed these predictions (Fig A in S4 Text). The assumption of no CO$_2$ gradient in the intercellular air space (ii) is reasonable for tomato leaves. The intercellular air space in tomato leaves are highly interconnected[17]. This high interconnectivity, combined with the fact that the diffusion coefficient of CO$_2$ in air is about 10^4 times as large as in water at room temperature[44], makes it very unlikely that there is a CO$_2$ gradient in the intercellular air space in tomato leaves or any other homobaric leaf with highly interconnected air space. This was demonstrated in [23], where a 3-D model was used to simulate CO$_2$ diffusion in both the intercellular air space and within mesophyll cells. There was only a stomatal pore modelled at the abaxial leaf surface. In [23] it was found that the CO$_2$ concentration difference between the upper and lower boundary was less than 0.1%. In order to discuss the impact of modelling a 2-D leaf structure (iii), instead of 3-D leaf structure, we will first discuss potential problems of a 2-D approach and then how we dealt with these issues. If a digitized transversal section of a leaf is used as a 2-D computational domain [45–47], it is implicitly assumed that S_m/S equals the length ratio of the exposed mesophyll surface area to the length of the section L_m/L, measured from leaf transversal sections. This assumption will result in the underestimation of the exposed mesophyll surface available for CO$_2$ uptake [48,49] and, thereby, the net CO$_2$ assimilation rate. In our model, we dealt with this issue by modelling the leaf as a rectangular geometry in two dimensions and assuming that each of the leaf anatomical parameters (t_{wall}, t_{cyt}, t_{str}, q, S_c/S_m, S_m/S) does not change in the direction of the third dimension. Another implicit assumption of a 2-D reaction model from a previous study [46] was that air spaces that seemed isolated in 2-D microscopic images from transversal leaf sections were also isolated in 3-D space. This makes the mesophyll surface exposed to these isolated air spaces unavailable for CO$_2$ uptake, which lowers the net CO$_2$ assimilation rate even more. In [46] study, the problem of assumed isolated intercellular air spaces and of the assumption that L_m/L was equal to S_m/S was solved by estimating the diffusion coefficients for CO$_2$ in the epidermis and the cell wall from gas exchange measurement data. This resulted in effective diffusion coefficients for CO$_2$ that were about 100 times as large as water. Although applying these effective diffusion coefficients resulted in a reasonable fit of gas exchange measurements with simulated A_N-C_i and A_N-I_{inc} curves, their concentration profiles show that the cell wall and the interface between the epidermal cells and the mesophyll cells are a major diffusion pathways for CO$_2$, which is very unlikely. In our 2-D model, the issue of isolated air spaces is solved by assuming that the resistance for CO$_2$ transport in the intercellular air space is negligible and by implementing stomatal conductance in the boundary conditions of the outer border of the computational domain. In S5 Text, we checked whether our other assumptions, namely, the reduction of the leaf structure to simple geometrical shapes (iv) and not explicitly modelling the light gradient (v) and carbonic anhydrase activity (vi), affect the predicted net CO$_2$ assimilation rate. We did so by comparing simulated $A - C_a$ curves modelled by a complex 3-D model that does not have any of these simplifications [28] with $A - C_a$ curves modelled by the

model from our study. The net CO_2 assimilation rates were about the same. All these analyses above show that the simplifications in our model, at least for tomato, do not affect the predictions of the net CO_2 assimilation rate.

There are analyses that cannot be done with the current version of the model, as they require more details on the description of the leaf geometry. Our previous study [28] examined to what extent C_3 leaf photosynthesis can be optimized by optimizing the gradient of photosynthetic capacity parameters (V_{cmax}, T_p and the maximum rate of electron transport J_{max}) between the upper and the lower epidermis. However, such an analysis requires huge computational times and a 3-D tomography of a leaf. In order to make such analyses less time and resource demanding, in future research it could be examined whether our simple 2-D model is capable of reproducing the results from[28]. This could be done, by instance, for defining the 2-D leaf geometry in the model, I_{inc}, J_{max}, V_{cmax}, and T_p at different depths, solving the model at each depth and calculate the whole leaf net CO_2 assimilation rate.

To the best of our knowledge, this study is the first attempt to directly assess how the localization of released CO_2 produced by (photo)respiration could affect both the net rate of CO_2 assimilation and re-assimilation. This is important, because previous resistance models [13,14,17,18,29,30] make implicit assumptions about the location of (photo)respiration or about the CO_2 gradients in the cytosol. Our study showed that it is unlikely that (photo)respiratory CO_2 release takes place in the outer cytosol and also that it is unlikely that there is no CO_2 gradient in the cytosol. In our analyses, we limited the number of scenarios to two extreme situations (all (photo)respiratory CO_2 release takes place in the outer cytosol or in the inner cytosol) and one intermediate situation. Recently, it has been shown that mitochondria can be present in both the inner and the outer half of the cytosol in C_3 grasses [50], which could explain differences in photosynthetic capacity among species. In future research, one could use the model presented in this study as a tool to analyse how the distribution of mitochondria over different cytosol compartments affects leaf photosynthesis.

Additionally, none of the aforementioned models allows to model CO_2 diffusion through the gaps between the chloroplasts. This can affect the predicted net CO_2 assimilation rate and fraction of (photo)respired CO_2 that is re-assimilated. Since the parameter estimates in our study are directly estimated by the model, for each estimate it is clear what the assumed location of (photo)respiration is. As far as the authors know, the only attempt in which a reaction diffusion model is directly used to estimate FvCB parameters is described in [26]. In that study, parameters for the FvCB model and parameters for the temperature response were estimated by both a 3-D model [23] and by a simple photosynthesis model [51]. In [26] it was found that the estimates can be quite different, because the 3-D model described in [23,26] is capable of partitioning the temperature response of photosynthesis due to physical (solubility of CO_2 in the liquid phase, temperature response of the diffusion coefficient of CO_2 in water) and biochemical (temperature dependency of kinetic constants of Rubisco) parameters.

Our model has the capability to distinguish how CO_2 transport is affected by biochemical processes and leaf structural barriers. Therefore it can be interesting to use the model in future research to re-examine the temperature response of various photosynthetic parameters. As our model is also capable of calculating the fraction of (photo)respired CO_2, it can also be used in further research to investigate how environmental conditions (C_a, I_{inc}, O, temperature) and stomatal conductance affect re-assimilation. It would further be interesting to further validate the model for other tomato cultivars and crop species and environmental conditions and subsequently investigate how this affects the re-assimilation of (photo)respired CO_2 and the estimates of photosynthetic parameters. Finally, the results of the validation of our 2-D model

suggest that it is possible to simplify both the structures and the processes, while the model still is capable of predicting the net CO_2 assimilation well.

Material and methods

Description of the experimental data

We used experimental data described in[17]. This data set consisted of microscopic and ultra-microscopic leaf anatomical measurements as well as simultaneous gas exchange and chlorophyll fluorescence measurements on leaves of two ages in three tomato cultivars. The gas exchange measurements consisted of CO_2 and light response measurements under both 21% O_2 and 2% O_2. For our present study, we only used the data for 15-days old leaves of cv. 'Admiro'. Those data can be found in S7 Text.

Description of the geometry of the model

The 2-D computational domain consists of an l x h rectangular section of a mesophyll cell exposed to the intercellular space. The centre of this section contains a single rectangular chloroplast with dimensions t_{str} x h_{str}. The remaining part of the section consists of cytosol. This cytosol compartment was subdivided into inner cytosol (rectangular cytosol layer adjacent to tonoplast), outer cytosol (rectangular cytosol layer adjacent to plasma membrane), and two remaining rectangles called cytosol gaps. The lengths of the inner and outer cytosol are $t_{cyt,inner}$ and $t_{cyt,outer}$. It is assumed (unless explicitly mentioned) that $t_{cyt,in} = t_{cyt,out} = t_{cyt}$. For reasons of symmetry, the height of the cytosol gap at the bottom and the top of the computational domain was half of that of the total gap height (h_{gap}). More details on the reconstruction of the geometry can be found in S1 Text. The chloroplast envelope was modelled as a thin film diffusion barrier. Since preliminary simulations showed that the presence of a vacuole did barely affect the net CO_2 assimilation rate, we did not include a vacuole. An insulated boundary condition (net flux is zero) was applied over the tonoplast, which is the membrane between the inner cytosol and the vacuole.

In all simulations an assumption from [27] was adopted; namely, the aspect ratio q of the chloroplasts (in this study, $q = \frac{t_{str}}{h_{str}}$) was constant and equal to 2.5. The gap width h_{gap} was varied in order to produce geometries with different values of S_c/S_m. It can be expressed as:

$$h_{gap} = qt_{str}\left(\left(\frac{S_c}{S_m}\right)^{-1} - 1\right) \tag{2}$$

More details on the derivation of Eq (2) can be found in S2 Text. By applying this geometry, it is assumed that all anatomical parameters (S_c/S_m, t_{str}, t_{cyt}, and q) are uniform in the paradermal direction.

Process description

Diffusion equation for CO_2 transport.   In a steady state, CO_2 diffusion, consumption and production should be in balance as:

$$\nabla \cdot D_{CO_{2,i}}\nabla[CO_2] = w_i - r_{p,i} - r_{d,i} \tag{3}$$

where the subscript 'i' denotes the medium (either a cytosol compartment or the stroma). $D_{CO_2,i}$ is the diffusion coefficient of CO_2 (m^2 s^{-1}) in compartment i. w_i is the volumetric rate of carboxylation by Rubisco (mol CO_2 m^{-3} s^{-1}), which is only non-zero in the stroma. $r_{p,i}$ is the volumetric rate of photorespiration (mol CO_2 m^{-3} s^{-1}), which is only non-zero in the cytosol.

r_d is the volumetric rate of respiration (mol CO_2 m^{-3} s^{-1}) that is only non-zero in the cytosol and was taken as a constant. [CO_2] is the CO_2 concentration (mol m^{-3}). ∇ (m^{-1}) is the gradient operator. The diffusion coefficient for CO_2 transport depends on the porosity and the viscosity of the medium. For the cytosol and the stroma, the diffusion coefficient for CO_2 was calculated as[29]:

$$D_{CO_2,i} = p_{eff,i}\zeta_i D_{CO_2,water} \tag{4}$$

where p_{eff} is the effective porosity of the medium. It was assumed that the effective porosity of the cytosol and the stroma is 1.0. ζ_i is a reduction factor in the medium compared to pure water due to a higher viscosity of the media compared to water and was assumed to be 0.5 for the stroma and the cytosol and 1.0 for the cell wall[17,28]. Table 1 shows values and units of physical parameters used in this study.

Carboxylation rate. The FvCB model[5], expanded with triose phosphate utilization limited carboxylation[52], was used to quantify the rate of carboxylation by Rubisco w in the stroma:

$$w = \min\left(\frac{[CO_2]v_{cmax}}{[CO_2] + k_{mC}\left(1 + \frac{[O_2]}{k_{mO}}\right)}, \frac{j[CO_2]}{4[CO_2] + 8\gamma^*}, \frac{3t_p}{1 - \frac{\gamma^*}{[CO_2]}}\right) \tag{5}$$

where v_{cmax} is the maximum volumetric rate of carboxylation by Rubisco (mol m^{-3} s^{-1}); k_{mC} and k_{mO} are the Michaelis-Menten constants of Rubisco (mol m^{-3}) for carboxylation and oxygenation, respectively; j is the volumetric rate of electron transport (mol m^{-3} s^{-1}); t_p is the volumetric rate of triose phosphate utilization (mol m^{-3} s^{-1}); and γ^* is the CO_2 compensation point, the CO_2 concentration (mol m^{-3}) in the stroma at which the amount of CO_2 consumed by carboxylation equals the amount of CO_2 released by photorespiration.

Photorespiration rate. The rate of CO_2 production due to photorespiration was modelled as[27]:

$$r_p = \left(\iint_{Stroma} \frac{\gamma^* w}{[CO_2]} dx\, dy\right)\left(\iint_{(Photo)respiration} dx\, dy\right)^{-1} \tag{6}$$

where "Stroma" is the stroma compartment in the computational domain, and "(Photo)respiration" is the location in the computational domain, in which CO_2 release by (photo)respiration is assumed to take place. Three different scenarios for the location for CO_2 release by (photo)respiration were considered: either (1) the inner cytosol, or (2) the outer cytosol, or (3) the cytosol gaps between the chloroplasts.

Unit conversions

The variables v_{cmax}, r_d, r_p, t_p, j and w in Eqs (3), (5) and (6) are rates per unit of volume. Their equivalents expressed in rate per unit of leaf area (mol m^{-2} s^{-1}) are denoted here in capitals; V_{cmax}, R_d, R_p, T_p, J and W. In order to calculate j, v_{cmax}, and t_p, J, V_{cmax} and T_p are multiplied with the ratio S/V_{str}, which is the ratio of the leaf area to the total volume of the stroma in a leaf. S2 Text and S3 Text explain how this term is derived mathematically; r_d is calculated by multiplying R_d with $S/V_{cyt,inner}$, $S/V_{cyt,outerr}$, or $S/V_{cyt,gap}$, depending on the scenario. Table 3 shows mathematical expressions for these surface to volume fractions.

There are also a number of parameters that represent concentrations (k_{mC}, k_{mO}, γ^*, [O_2], [CO_2]) expressed in mol m^{-3}. In most photosynthesis research, these parameters are expressed as partial pressures instead (here written as K_{mC}, K_{mO}, Γ^*, O). The ideal gas law and Henry's

Table 3. Overview of surface to volume ratios and parameterizations.

Symbol	Unit	Mathematical expression	Meaning of ratios
$\frac{S}{V_{str}}$	m^{-1}	$\frac{1}{t_{str}} \left(\frac{S_m}{S} \right)^{-1} \left(\frac{S_c}{S_m} \right)^{-1}$	Leaf area to total chloroplast volume
$\frac{S}{V_{cyt,inner}}$	m^{-1}	$\frac{1}{t_{cyt}} \left(\frac{S_m}{S} \right)^{-1}$	Leaf area to total volume of the inner cytosol
$\frac{S}{V_{cyt,outer}}$	m^{-1}	$\frac{1}{t_{cyt}} \left(\frac{S_m}{S} \right)^{-1}$	Leaf area to total volume of the outer cytosol
$\frac{S}{V_{cyt,gap}}$	m^{-1}	$\frac{1}{t_{str}} \left(\frac{S_m}{S} \left(1 - \frac{S_c}{S_m} \right) \right)^{-1}$	Leaf area to total volume of the cytosol gaps

https://doi.org/10.1371/journal.pone.0183746.t003

law were applied [53] to convert all mentioned CO_2 partial pressure parameters, expressed in gas phase (K_{mC}, K_{mO}, Γ^*), into concentrations in the liquid phase.

Quantification of parameters

Quantification of leaf anatomical parameters. Leaf anatomical parameters (t_{cyt}, t_{str}, S_c/S_m, S_m/S, t_{wall}) for 15-day-old Admiro leaves were adopted from [17]. S_c/S_m, t_{cyt}, and t_{str} were used to generate a unique geometry for this leaf, as described in S1 Text, S2 Text and S3 Text. The anatomical parameter values are listed in Table 1. The measured cytosol thicknesses are considerably smaller than the thickness of mitochondria assumed in [27]. To the best of our knowledge, there have been no systematic measurements of diameters of mitochondria and some sample images from a number of studies [20,54,55] suggest that this diameter can vary considerably. Due to lack of data, we assumed that the thickness is equal to the cytosol thickness measured on the TEM images in [17]. In S6 Text, we present a sensitivity analysis for $t_{cyt, inner}$ and $t_{cyt,outer}$ to show that these thicknesses have a very small effect on A_N and f_{rec}.

Quantification of Rubisco kinetic parameters. We adopted the Michaelis-Menten constants for carboxylation (K_{mC}) and oxygenation (K_{mO}) by Rubisco from [28]. We further assumed that the specificity factor of Rubisco for CO_2 and O_2, $S_{C/O}$, equals 2.6 [14]. For $S_{C/O}$, we calculated the CO_2 compensation point Γ^* as:

$$\Gamma^* = \frac{0.5O}{S_{C/O}} \quad (7)$$

Determination of the rate of electron transport. We used $A_N - I_{inc}$ data measured at 2% O_2 under limiting irradiance conditions (I_{inc} equal to 25, 50, 100, and 150 µmol m^{-2} s^{-1}) to fit A_N against $\frac{1}{4}\Phi_2 I_{inc}$ by linear regression, where Φ_2 is the quantum yield of Photosystem II derived from chlorophyll fluorescence measurements [56]. Based on the estimated slope of this regression (s), we calculated the rate of electron transport J for each combination of averages of the measured values for I_{inc} and Φ_2 as in [13]:

$$J = s\Phi_2 I_{inc} \quad (8)$$

Fig A in S8 Text shows the relationship between J and I_{inc}.

Boundary conditions

In the model, it is assumed that the resistance of the intercellular air space for CO_2 transport is negligible. The cell wall and the plasma membrane were not modelled as separate domains, because they were very thin. Together with the stomata, they were incorporated in the

boundary conditions of the combined cell wall and plasma membrane (Fig 2) instead. The following convection boundary conditions were thus assigned to these edges:

$$\phi_{wp} = \frac{1}{\frac{1}{G_s} + \frac{t_{wall}}{p_{eff,wall}D_{CO_2,water}} + \frac{1}{G_{mem}}} \left(\frac{RT}{H}[CO_2]_a - [CO_2]_l \right) \tag{9}$$

where ϕ_{wp} is the net flux of CO$_2$ over the cell wall from the intercellular air space normal to the mesophyll surface; $[CO_2]_a$ is the CO$_2$ concentration at the leaf surface; $[CO_2]_l$ is the local liquid phase CO$_2$ concentration at the mesophyll surface; G_{mem} is the plasma membrane conductance (m s^{-1}); t_{wall} is the cell wall thickness; p_{eff} is the effective porosity of the cell wall; R is the universal gas constant; T is the temperature; and H is Henry's law constant for CO$_2$ at temperature T and standard pressure. The term RT/H represents the dimensionless Henry's law constant that is used to convert gas phase concentrations into liquid phase concentrations [29,53]. It is assumed that $G_{mem} = 3.5 \cdot 10^{-3}$ m s^{-1} [17] and $p_{eff,wall} = 0.2$. G_s represents the stomatal conductance expressed in m s^{-1}. It was calculated from the measured stomatal conductance, expressed in mol m^{-2} s^{-1} Pa^{-1}, as:

$$G_s = g_s \left(\frac{S_m}{S} \right)^{-1} RT \tag{10}$$

Since the chloroplast envelope is a double membrane, it was assumed that its conductance was half that of the plasma membrane. Therefore, the flux over the chloroplast envelope was modelled as a resistance with conductance $G_{env} = \frac{1}{2}G_{mem}$. By applying Eqs (9) and (10), it was assumed that the resistance of the intercellular air space was negligible. All other boundaries of the computational domain were insulated as explained earlier. The formulation of the boundary conditions was equal for any of the scenarios for the location of mitochondria.

Estimation of leaf physiological parameters

We used the reaction-diffusion model directly to estimate the parameters R_d and V_{cmax} by minimizing the squared difference between the model and the data. For both estimation procedures, we used the MATLAB (The Mathworks, Natick, USA) lsqnonlin() function. We calculated the standard error of these estimates as $\sqrt{v \cdot \text{diag}(\mathbf{J^T} \cdot \mathbf{J})^{-1}}/n$, where v is the squared norm of the residuals, $\mathbf{J}$ is the Jacobian matrix and $\mathbf{J^T}$ is the transposed Jacobian matrix, and n is the number of data points[57]. The data that were used for the estimation of R_d and V_{cmax} can be found in S7 Text.

Estimation of R_d. We estimated R_d, based on the assumed location of (photo)respiratory CO$_2$ release (inner cytosol, outer cytosol, or cytosol gaps between chloroplasts). For this estimation, we only used the A_N and g_s measurements from A_N-I_{inc} curve measurements at I_{inc} set at 25, 50, 100, and 150 μmol m^{-2} s^{-1} at $O = 21$ kPa and $C_a = 40$ Pa. For this range of light levels, corresponding to limiting light levels commonly used to estimate R_d by conventional methods (12,38,40,41), we estimated R_d by minimizing the squared difference between average measured net rates of CO$_2$ assimilation and the ones for each light level simulated by the reaction-diffusion model. For these light levels, the RuBP carboxylation rate is always limited by electron transport; so, R_d is expected to be estimated using J and Γ^* as inputs.

Determination of T_p. In order to calculate T_p, we first determined the triose-phosphate-utilization-limited net CO$_2$ assimilation rate A_p as the average measured net CO$_2$ assimilation rate at $C_a = 200$ Pa, $O = 21$ kPa and $I_{inc} = 1500$ μmolm^{-2} s^{-1}. From that average net CO$_2$

assimilation rate, we calculated T_p as:

$$T_p = \frac{(A_p + R_d)}{3} \qquad (11)$$

where we used the previously estimated values of R_d as input for Eq (11). By doing so, we made the assumption that, for these conditions of very high light and ambient CO_2 levels, photosynthesis is limited only by triose-phosphate limitations throughout the chloroplast.

Estimation of V_{cmax}. For the estimation of V_{cmax}, we only used the A_N and C_i measurements from A_N-C_i curves measured at $I_{inc} = 1500$ μmol m^{-2} s^{-1}, $O = 21$ kPa and C_a equal to 5, 10, 15, and 20 Pa. We estimated V_{cmax} by minimizing the squared difference between the average measured and simulated net CO_2 assimilation rates at these ambient CO_2 levels, assuming that the net CO_2 assimilation rate is limited by Rubisco. During this procedure, we used the previously determined values for R_d and T_p as input variables. In order to do this estimation, we used COMSOL 5.2a with MATLAB livelink (COMSOL AB, Stockholm, Sweden) to convert the COMSOL model into a MATLAB 2014b (The Mathworks, Natick, USA) script to allow optimization. S11 Text contains scripts for the scenario that assumes (photo)respired CO_2 release in the inner cytosol (Script A in S11 Text), the outer cytosol (Script B in S11 Text) and the cytosol gaps (Script C in S11 Text), respectively.

Validation

We did not use the measurements of the A_N-C_i curves at ambient CO_2 levels if the leaf was exposed to CO_2 partial pressures between 40 Pa and 160 Pa for the estimation of s, R_d, T_p, and V_{cmax}. Neither did we use the A_N-I_{inc} measurements at irradiances between 300 and 1500 μmol m^{-2} s^{-1}. We used these remaining combinations of measured values for O, I_{inc}, and C_i to predict the net CO_2 assimilation rate and compared these predictions with the experimental data. Those data can be found in S7 Text. We also checked whether a model with a single CO_2 pool and two CO_2 pools ($^{12}CO_2$ and $^{13}CO_2$) would result in the same results. For each scenario, the calculated values for C_c, C_i and f_{rec} were the same.

Solving the model and post-processing. The model was implemented and solved in the finite element software COMSOL Multiphysics 5.1. After solving the model, the rate of CO_2 production by RuBP carboxylation rate W, expressed as the rate per unit of leaf area per second, was calculated by multiplying the average volumetric rate of RuBP carboxylation by the total stroma volume and dividing this by the leaf surface area:

$$W = \left(\frac{S}{V_{str}}\right)^{-1} \left(\iint_{Stroma} w \, dx \, dy\right) \left(\iint_{Stroma} dx \, dy\right)^{-1} \qquad (12)$$

The rate of CO_2 production per unit of leaf area by photorespiration was calculated as:

$$R_p = \left(\frac{S}{V_{str}}\right)^{-1} \left(\iint_{Stroma} \frac{w\gamma^*}{[CO_2]} \, dx \, dy\right) \left(\iint_{Stroma} dx \, dy\right)^{-1} \qquad (13)$$

The net rate of CO_2 assimilation was calculated as:

$$A_N = W - R_p - R_d \qquad (14)$$

We used the calculated net CO_2 assimilation rate and the simulated CO_2 gradient in the chloroplast stroma to calculate the average CO_2 partial pressure in the air spaces and the

chloroplast stroma C_c, expressed in the gas phase, as:

$$C_i = C_a - \frac{A_N}{g_s} \tag{15}$$

$$C_c = H \left(\iint_{\text{Stroma}} [CO_2] \right) \left(\iint_{\text{Stroma}} dx\, dy \right)^{-1} \tag{16}$$

Estimating re-assimilation of (photo)respired CO2

The model was used to calculate the fraction (f_{rec}) of CO_2 produced by (photo)respiration that is re-assimilated. The method to achieve this is largely based on the method described in [28]. We used our model to conduct an *in silico* experiment mimicking the *in vivo* experiment described in[38]. In this experiment, a leaf was adapted to ambient CO_2 levels and saturating light. Under ambient conditions, atmospheric CO_2 mainly consists of $^{12}CO_2$ isotopes. After adaptation, the leaf was exposed to air that contained $^{13}CO_2$, but no $^{12}CO_2$. The concentration of $^{13}CO_2$ was the same as the concentration of $^{12}CO_2$ under ambient conditions. The concentrations of $^{12}CO_2$ and $^{13}CO_2$ at the leaf surface reached new equilibrium concentrations after about 12 seconds. Although no atmospheric $^{12}CO_2$ is taken up, the assimilates still contain mainly ^{12}C isotopes, so all CO_2 produced by (photo)respiration consists of $^{12}CO_2$. It takes a longer period (20–30 s) than the 12-seconds adaptation time before measureable amounts of $^{13}CO_2$ are released by (photo)respiration. The authors of this study [38] exploited this fact by stating that $^{12}CO_2$ and $^{13}CO_2$ are in quasi steady state during this period of 12 seconds. Since all (photo)respired CO_2 consists of $^{12}CO_2$, the measured net $^{13}CO_2$ assimilation rate $^{13C}A_N$ equals the carboxylation rate W. Next they measured the $^{12}CO_2$ and $^{13}CO_2$ concentrations in the intercellular air space. The total CO_2 concentration ($^{12}[CO_2] + [^{13}CO_2]$) is during the experiment. Since the discrimination of $^{13}CO_2$ is very small (0.27‰) [58], they therefore assumed it to be negligible and stated that: $^{12}A_N = \frac{[^{12}CO_2]_i}{[^{13}CO_2]_i} {}^{13}A_N$.

The symbols $[^{12}CO_2]_i$ and $[^{13}CO_2]_i$ represent the concentrations of $^{12}CO_2$ and $^{13}CO_2$, respectively, in the intercellular air space. Since all assimilated CO_2 produced by (photo)respiration consists of $^{12}CO_2$, $^{12}A_N$ is also the rate of CO_2 re-assimilation.

For the *in silico* experiment in this study, Eq (3) was replaced by separate reaction-diffusion equations for $^{12}CO_2$ and $^{13}CO_2$ transport. Since all CO_2 production by (photo)respiration consists of $^{12}CO_2$, the partial differential equations for $^{12}CO_2$ and $^{13}CO_2$ can be expressed as:

$$\nabla \cdot D_{CO_2,i} \nabla [^{12}CO_2] = w_{12} - r_d - r_p \tag{17}$$

$$\nabla \cdot D_{CO_2,i} \nabla [^{13}CO_2] = w_{13} \tag{18}$$

Since the total CO_2 concentration does not change after $^{12}CO_2$ in the air near the leaf surface was replaced by $^{13}CO_2$, $^{12}[CO_2] + [^{13}CO_2]$ were substituted for $[CO_2]$ in Eqs (5) and (6). The volumetric consumption of $^{12}CO_2$ and $^{13}CO_2$ by RuBP carboxylation (w_{12} and w_{13}) were

expressed as:

$$w_{12} = \frac{[^{12}\text{CO}_2]}{[^{12}\text{CO}_2] + [^{13}\text{CO}_2]} w \tag{19}$$

$$w_{13} = \frac{[^{13}\text{CO}_2]}{[^{12}\text{CO}_2] + [^{13}\text{CO}_2]} w \tag{20}$$

It is assumed that the $^{12}\text{CO}_2$ concentration at the leaf surface is zero and the following conditions were applied at the mesophyll cell surface, in analogy to Eq (9):

$$\phi_{\text{wp},^{12}\text{CO}_2} = -\frac{1}{\frac{1}{G_s} + \frac{t_{\text{wall}}}{p_{\text{eff,wall}} D_{\text{CO}_2,\text{water}}} + \frac{1}{G_{\text{mem}}}} [^{12}\text{CO}_2]_l \tag{21}$$

$$\phi_{\text{wp},^{13}\text{CO}_2} = \frac{1}{\frac{1}{G_s} + \frac{t_{\text{wall}}}{p_{\text{eff,wall}} D_{\text{CO}_2,\text{water}}} + \frac{1}{G_{\text{mem}}}} \left(\frac{RT}{H} [^{13}\text{CO}_2]_a - [^{13}\text{CO}_2]_l \right) \tag{22}$$

where $\phi_{\text{wp},^{12}\text{CO}_2}$ and $\phi_{\text{wp},^{13}\text{CO}_2}$ are the net fluxes of $^{12}\text{CO}_2$ and $^{13}\text{CO}_2$ respectively over the stomata, the intercellular air space, the cell wall and the plasma membrane; $[^{13}\text{CO}_2]_a$ is the concentration of $^{13}\text{CO}_2$ at the leaf surface.

The re-assimilation rate was calculated, equivalent to the rate $^{12}\text{CO}_2$ consumption due to RuBP carboxylation W_{12}, as:

$$W_{12} = \left(\frac{S}{V_{\text{str}}} \right)^{-1} \left(\iint_{\text{Stroma}} w_{12} \, dx \, dy \right) \left(\iint_{\text{Stroma}} dx \, dy \right)^{-1} \tag{23}$$

We validated the extension of the model with two CO_2 isotopes by comparing C_c, f_{rec} and C_i calculated by this model and by the model that assumes only one CO_2 pool for each scenario. The fraction of CO_2 produced by (photo)respiration that is re-assimilated is calculated as[28]:

$$f_{\text{rec}} = \frac{W_{12}}{R_d + R_p} \tag{24}$$

Note that our definition of re-assimilation is different from the one from[38]. In our study, we define the rate of re-assimilation as the rate of $^{12}\text{CO}_2$ RuBP carboxylation W_{12}. In contrast, in the definition of the rate of re-assimilation in [38] is $\frac{[^{12}\text{CO}_2]_i}{[^{13}\text{CO}_2]_i} {}^{13}A_N$, it is assumed that the rate of intracellular re-assimilation is negligible [20]. Therefore, this rate is called the rate of intercellular respiration in [20], which is the rate at which (photo)respired CO_2 that enters the intercellular air spaces is re-assimilated. In this definition of intercellular respiration, it is implicitly assumed that RuBP carboxylation and (photo)respiration take place in the same compartment. As our model takes into account that (photo)respiration takes place in different compartments, this definition of intercellular re-assimilation cannot be used in our model. Therefore, we did not explicitly intercellular re-assimilation rates in our model.

Additional analyses

S4 Text contains the description of a sensitivity analysis for $t_{\text{cyt,in}}$ and $t_{\text{cyt,out}}$ to assess how these parameters may affect A_N and f_{rec}. S4 Text also describes an analysis in which the

mitochondria were modelled explicitly to assess to what extent modelling loose mitochondria may change the calculated values of A_N and f_{rec}.

Supporting information

S1 Text. Construction of the 2-D computational domain.
(DOCX)

S2 Text. Parameterization of the 2-D computational domain.
(DOCX)

S3 Text. Parameterization of volume to volume and area to volume ratios.
(DOCX)

S4 Text. Modelling individual mitochondrial compartments.
(DOCX)

S5 Text. The impact of simplifications in the leaf geometry and transport processes on A_N and f_{rec}.
(DOCX)

S6 Text. Sensitivity analysis of f_{rec} and A_N to $t_{cyt,in}$ and $t_{cyt,out}$.
(DOCX)

S7 Text. Experimental data simultaneous gas exchange and chlorophyll fluorescence measurements.
(DOCX)

S8 Text. Calculation of the rate of electron transport.
(DOCX)

S9 Text. Sensitivity analysis estimate V_{cmax} to R_d.
(DOCX)

S10 Text. SAS code estimation V_{cmax}.
(DOCX)

S11 Text. MATLAB with COMSOL 5.2 source codes.
(DOCX)

Acknowledgments

Author Contributions

Conceptualization: Herman N. C. Berghuijs, Xinyou Yin, Q. Tri Ho, Bart M. Nicolaï, Paul C. Struik.

Data curation: Herman N. C. Berghuijs, Xinyou Yin, Pieter Verboven, Paul C. Struik.

Formal analysis: Xinyou Yin, Q. Tri Ho, Moges A. Retta.

Funding acquisition: Herman N. C. Berghuijs, Xinyou Yin, Paul C. Struik.

Investigation: Herman N. C. Berghuijs, Xinyou Yin, Q. Tri Ho, Moges A. Retta, Paul C. Struik.

Methodology: Herman N. C. Berghuijs, Xinyou Yin, Q. Tri Ho, Moges A. Retta, Pieter Verboven, Bart M. Nicolaï, Paul C. Struik.

Project administration: Xinyou Yin, Bart M. Nicolaï, Paul C. Struik.

Resources: Herman N. C. Berghuijs, Xinyou Yin, Pieter Verboven, Paul C. Struik.

Software: Herman N. C. Berghuijs, Q. Tri Ho, Moges A. Retta, Pieter Verboven.

Supervision: Xinyou Yin, Pieter Verboven, Bart M. Nicolaï, Paul C. Struik.

Validation: Herman N. C. Berghuijs, Q. Tri Ho, Bart M. Nicolaï.

Visualization: Herman N. C. Berghuijs, Q. Tri Ho.

Writing – original draft: Herman N. C. Berghuijs, Xinyou Yin, Q. Tri Ho, Moges A. Retta, Bart M. Nicolaï, Paul C. Struik.

Writing – review & editing: Herman N. C. Berghuijs, Xinyou Yin, Q. Tri Ho, Moges A. Retta, Pieter Verboven, Bart M. Nicolaï, Paul C. Struik.

References

1. Flexas J, Ribas-Carbo M, Diaz-Espejo A, Galmes J, Medrano H (2008) Mesophyll conductance to CO_2: current knowledge and future prospects. Plant Cell and Environment 31: 602–621.

2. Flexas J, Barbour MM, Brendel O, Cabrera HM, Carriqui M, et al. (2012) Mesophyll diffusion conductance to CO_2: An unappreciated central player in photosynthesis. Plant Science 193–194: 70–84. https://doi.org/10.1016/j.plantsci.2012.05.009 PMID: 22794920

3. Harley PC, Loreto F, Dimarco G, Sharkey TD (1992) Theoretical considerations when estimating the mesophyll conductance to CO_2 flux by analysis of the response of photosynthesis to CO_2. Plant Physiology 98: 1429–1436. PMID: 16668811

4. Niinemets U, Diaz-Espejo A, Flexas J, Galmes J, Warren CR (2009) Importance of mesophyll diffusion conductance in estimation of plant photosynthesis in the field. Journal of Experimental Botany 60: 2271–2282. https://doi.org/10.1093/jxb/erp063 PMID: 19305021

5. Farquhar GD, Caemmerer SV, Berry JA (1980) A biochemical model of photosynthetic CO_2 assimilation in leaves of C_3 species. Planta 149: 78–90. https://doi.org/10.1007/BF00386231 PMID: 24306196

6. Pons TL, Flexas J, von Caemmerer S, Evans JR, Genty B, et al. (2009) Estimating mesophyll conductance to CO2: methodology, potential errors, and recommendations. Journal of Experimental Botany 60: 2217–2234. https://doi.org/10.1093/jxb/erp081 PMID: 19357431

7. Berghuijs HNC, Yin X, Ho QT, Driever SM, Retta MA, et al. (2016) Mesophyll conductance and reaction-diffusion models for CO_2 transport in C_3 leaves; needs, opportunities and challenges. Plant Science 252: 62–75. https://doi.org/10.1016/j.plantsci.2016.05.016 PMID: 27717479

8. Flexas J, Diaz-Espejo A, Galmes J, Kaldenhoff R, Medrano H, et al. (2007) Rapid variations of mesophyll conductance in response to changes in CO_2 concentration around leaves. Plant Cell and Environment 30: 1284–1298.

9. Yin X, Struik PC (2009) Theoretical reconsiderations when estimating the mesophyll conductance to CO_2 diffusion in leaves of C_3 plants by analysis of combined gas exchange and chlorophyll fluorescence measurements. Plant Cell and Environment 32: 1513–1524.

10. Gu LH, Sun Y (2014) Artefactual responses of mesophyll conductance to CO2 and irradiance estimated with the variable J and online isotope discrimination methods. Plant Cell and Environment 37: 1231–1249.

11. Leuning R (1995) A critical-appraisal of a combined stomatal-photosynthesis model for C$_3$ plants. Plant Cell and Environment 18: 339–355.

12. Gu JF, Yin X, Stomph TJ, Wang HQ, Struik PC (2012) Physiological basis of genetic variation in leaf photosynthesis among rice (Oryza sativa L.) introgression lines under drought and well-watered conditions. Journal of Experimental Botany 63: 5137–5153. https://doi.org/10.1093/jxb/ers170 PMID: 22888131

13. Yin X, Struik PC, Romero P, Harbinson J, Evers JB, et al. (2009) Using combined measurements of gas exchange and chlorophyll fluorescence to estimate parameters of a biochemical C$_3$ photosynthesis model: a critical appraisal and a new integrated approach applied to leaves in a wheat (Triticum aestivum) canopy. Plant Cell and Environment 32: 448–464.

14. Tholen D, Ethier G, Genty B, Pepin S, Zhu XG (2012) Variable mesophyll conductance revisited: theoretical background and experimental implications. Plant Cell and Environment 35: 2087–2103.

15. von Caemmerer S (2013) Steady-state models of photosynthesis. Plant Cell and Environment 36: 1617–1630.

16. Yin X, Struik PC (2017) Simple generalisation of a mesophyll resistance model for various intracellular arrangements of chloroplasts and mitochondria in C$_3$ leaves. Photosynthesis Research 132: 211–220. https://doi.org/10.1007/s11120-017-0340-8 PMID: 28197891

17. Berghuijs HNC, Yin X, Ho QT, van der Putten PEL, Verboven P, et al. (2015) Modelling the relationship between CO$_2$ assimilation and leaf anatomical properties in tomato leaves. Plant Science 238: 297–311. https://doi.org/10.1016/j.plantsci.2015.06.022 PMID: 26259196

18. Tholen D, Ethier G, Genty B (2014) Mesophyll conductance with a twist. Plant Cell and Environment 37: 2456–2458

19. Sage TL, Sage RF (2009) The functional anatomy of rice leaves:implications for refixation of photorespiratory CO$_2$ and efforts to engineer C$_4$ photosynthesis into rice. Plant and Cell Physiology 50: 756–772. https://doi.org/10.1093/pcp/pcp033 PMID: 19246459

20. Busch FA, Sage TL, Cousins AB, Sage RF (2013) C$_3$ plants enhance rates of photosynthesis by reassimilating photorespired and respired CO$_2$. Plant Cell and Environment 36: 200–212.

21. Parkhurst DF (1977) A three-dimensional model for CO$_2$ uptake by continuously distributed mesophyll in leaves. Journal of Theoretical Biology 67: 471–488. PMID: 904326

22. Parkhurst DF, Mott KA (1990) Intercellular diffusion limits to CO$_2$ uptake in leaves. Plant Physiology 94: 1024–1032. PMID: 16667792

23. Aalto T, Juurola E (2002) A three-dimensional model of CO$_2$ transport in airspaces and mesophyll cells of a silver birch leaf. Plant Cell and Environment 25: 1399–1409.

24. Vesala T, Ahonen T, Hari P, Krissinel E, Shokhirev N (1996) Analysis of stomatal CO$_2$ uptake by a three-dimensional cylindrically symmetric model. New Phytologist 132: 235–245.

25. Aalto T, Vesala T, Mattila T, Simbierowicz P, Hari P (1999) A three-dimensional stomatal CO$_2$ exchange model including gaseous phase and leaf mesophyll separated by irregular interface. Journal of Theoretical Biology 196: 115–128. https://doi.org/10.1006/jtbi.1998.0820 PMID: 9892560

26. Juurola E, Aalto T, Thum T, Vesala T, Hari P (2005) Temperature dependence of leaf-level CO$_2$ fixation: revising biochemical coefficients through analysis of leaf three-dimensional structure. New Phytologist 166: 205–215. https://doi.org/10.1111/j.1469-8137.2004.01317.x PMID: 15760364

27. Tholen D, Zhu XG (2011) The mechanistic basis of internal conductance: a theoretical analysis of mesophyll cell photosynthesis and CO$_2$ diffusion. Plant Physiology 156: 90–105. https://doi.org/10.1104/pp.111.172346 PMID: 21441385

28. Ho QT, Berghuijs HNC, Watte R, Verboven P, Herremans E, et al. (2016) Three-dimensional microscale modelling of CO$_2$ transport and light propagation in tomato leaves enlightens photosynthesis. Plant, Cell and Environment 39: 50–61. https://doi.org/10.1111/pce.12590 PMID: 26082079

29. Tosens T, Niinemets U, Westoby M, Wright IJ (2012) Anatomical basis of variation in mesophyll resistance in eastern Australian sclerophylls: news of a long and winding path. Journal of Experimental Botany 63: 5105–5119. https://doi.org/10.1093/jxb/ers171 PMID: 22888123

30. Tomas M, Flexas J, Copolovici L, Galmes J, Hallik L, et al. (2013) Importance of leaf anatomy in determining mesophyll diffusion conductance to CO2 across species: quantitative limitations and scaling up by models. Journal of Experimental Botany 64: 2269–2281. https://doi.org/10.1093/jxb/ert086 PMID: 23564954

31. Kok B (1948) A critical consideration of the quantum yield of Chlorella photosynthesis. Enzymologia 13: 1–56.

32. Kok B (1949) On the interrelation of respiration and photosynthesis in green plates. Biochimica et Biophysica Acta 3: 625–631.

33. Laisk A (1977) Kinetics of photosynthesis and photorespiration in C3 plants (in Russian). Nauka Moscow.

34. Yin X, Sun ZP, Struik PC, Gu JF (2011) Evaluating a new method to estimate the rate of leaf respiration in the light by analysis of combined gas exchange and chlorophyll fluorescence measurements. Journal of Experimental Botany 62: 3489–3499. https://doi.org/10.1093/jxb/err038 PMID: 21382918

35. Parnik T, Keerberg O (2007) Advanced radiogasometric method for the determination of the rates of photorespiratory and respiratory decarboxylations of primary and stored photosynthates under steady-state photosynthesis. Physiologia Plantarum 129: 34–44.

36. Ethier GJ, Livingston NJ (2004) On the need to incorporate sensitivity to CO2 transfer conductance into the Farquhar-von Caemmerer-Berry leaf photosynthesis model. Plant Cell and Environment 27: 137–153.

37. Walker BJ, Skabelund DC, Busch FA, Ort DR (2016) An improved approach for measuring the impact of multiple CO2 conductances on the apparent photorespiratory CO2 compensation point through slope-intercept regression. Plant Cell Environ 39: 1198–1203. https://doi.org/10.1111/pce.12722 PMID: 27103099

38. Haupt-Herting S, Klug K, Fock HP (2001) A new approach to measure gross CO2 fluxes in leaves. Gross CO2 assimilation, photorespiration, and mitochondrial respiration in the light in tomato under drought stress. Plant Physiol 126: 388–396. PMID: 11351101

39. Loreto F, Delfine S, Di Marco G (1999) Estimation of photorespiratory carbon dioxide recycling during photosynthesis. Australian Journal of Plant Physiology 26: 733–736.

40. Terashima I, Hanba YT, Tazoe Y, Vyas P, Yano S (2006) Irradiance and phenotype: comparative eco-development of sun and shade leaves in relation to photosynthetic CO2 diffusion. Journal of Experimental Botany 57: 343–354. https://doi.org/10.1093/jxb/erj014 PMID: 16356943

41. Fanta SW, Vanderlinden W, Abera MK, Verboven P, Karki R, et al. (2012) Water transport properties of artificial cell walls. Journal of Food Engineering 108: 393–402.

42. Evans JR, Kaldenhoff R, Genty B, Terashima I (2009) Resistances along the CO$_2$ diffusion pathway inside leaves. Journal of Experimental Botany 60: 2235–2248. https://doi.org/10.1093/jxb/erp117 PMID: 19395390

43. Watté R, Aernouts B, Van Beers R, Herremans E, Ho QT, et al. (2015) Modeling the propagation of light in realistic tissue structures with MMC-fpf: a meshed Monte Carlo method with free phase function. Optics Express 23: 17467–17486. https://doi.org/10.1364/OE.23.017467 PMID: 26191756

44. Nobel PS (2009) Physicochemical and Environmental Plant Physiology. Oxford, United Kingdom: Elsevier Inc.

45. Pachepsky LB, Haskett JD, Acock B (1995) A two-dimensional model of leaf gas exchange with special reference to leaf anatomy. Journal of Biogeography 22: 209–214.

46. Ho QT, Verboven P, Yin X, Struik PC, Nicolai BM (2012) A microscale model for combined CO$_2$ diffusion and photosynthesis in leaves. Plos One 7.

47. Retta M, Ho QT, Yin X, Verboven P, Berghuijs HNC, et al. (2016) A two-dimensional microscale model of gas exchange during photosynthesis in maize (Zea mays L.) leaves. Plant Science 246: 37–51. https://doi.org/10.1016/j.plantsci.2016.02.003 PMID: 26993234

48. Evans JR, Von Caemmerer S, Setchell BA, Hudson GS (1994) The relationship between CO$_2$ transfer conductance and leaf anatomy in transgenic tobacco with a reduced content of Rubisco. Australian Journal of Plant Physiology 21: 475–495.

49. Thain JF (1983) Curvature correction factors in the measurement of cell-surface areas in plant-tissues. Journal of Experimental Botany 34: 87–94.

50. Hatakeyama Y, Ueno O (2016) Intracellular position of mitochondria and chloroplasts in bundle sheath and mesophyll cells of C$_3$ grasses in relation to photorespiratory CO$_2$ loss. Plant Production Science 19: 540–551.

51. Aalto T, Juurola E (2001) Parametrization of a biochemical CO2 exchange model for birch (Betula pendula Roth.). Boreal Environment Research 6: 53–64.

52. Sharkey TD (1985) Photosynthesis in intact leaves of C$_3$ plants—Physics, physiology and rate limitations. Botanical Review 51: 53–105.

53. Ho QT, Verboven P, Verlinden BE, Nicolai BM (2010) A model for gas transport in pear fruit at multiple scales. Journal of Experimental Botany 61: 2071–2081. https://doi.org/10.1093/jxb/erq026 PMID: 20194925

54. Gielwanowska I, Pastorczyk M, Kellmann-Sopyla W, Gorniak D, Gorecki RJ (2015) Morphological and ultrastructural changes of organelles in leaf mesophyll cells of the Arctic and Antarctic plants of Poaceae family under cold influence. Arctic Antarctic and Alpine Research 47: 17–25.

55. Moser T, Holzinger A, Buchner O (2015) Chloroplast protrusions in leaves of Ranunculus glacialisL. respond significantly to different ambient conditions, but are not related to temperature stress. Plant Cell and Environment 38: 1347–1356.

56. Genty B, Briantais JM, Baker NR (1989) The relationship between the quantum yield of photosynthetic electron-transport and quenching of chlorophyll fluorescence. Biochimica et Biophysica Acta 990: 87–92.

57. Van Riel N Parameter estimation in non-equidistantly sampled nonlinear state space models; a Matlab implementation

58. Farquhar GD, Oleary MH, Berry JA (1982) On the relationship between carbon isotope discrimination and the inter-cellular carbon-dioxide concentration in leaves. Australian Journal of Plant Physiology 9: 121–137.